Supplementary Material for

Metasurface-enabled quantum holograms with hybrid entanglement

Hong Liang,[a,†] Wai Chun Wong,[a,b,†] Tailin An,[a] and Jensen Li[a,b,*]

[a]*Department of Physics, The Hong Kong University of Science and Technology, Clear Water Bay, Kowloon, Hong Kong, 999077, P. R. China*

[b]*Department of Engineering, University of Exeter, EX4 4QF, UK*

† *These authors contributed equally to this work.*

* *jensenli@ust.hk*

This PDF file includes

Supplementary Text

Supplementary Figure S1 to S3

1. Materials and Methods

Sample fabrication

The dielectric metasurfaces were fabricated on a quartz substrate following the processes of deposition, patterning, and etching. First, a 300 nm polycrystalline silicon (Poly-Si) film was deposited by low-pressure chemical vapor deposition (LPCVD). The inverse nanostructures were patterned using an E-Beam lithography system (JEOL JBX-6300FS) within 200 nm electron beam resist (CSAR 6200.09), followed by baking at 150℃ for 1 minute. Finally, the desired structures were etched using SF6 and C4F8 in an inductively coupled plasma reactive-ion etching process (ICP-RIE).

Quantum optical measurement

In the experiment, we use a 2-mm-thick type-II BBO and a 200mW 405 nm laser (CrystaLaser DL-405-400) to generate the polarization-entangled photon pairs in a state of $(|L\rangle_{\mathrm{i}}|L\rangle_{\mathrm{s}} - |R\rangle_{\mathrm{i}}|R\rangle_{\mathrm{s}})/\sqrt{2}$. The half-opening angle of the generated photon pairs is designed to be 3°. The photons are split into the signal arm and idler arm using a prism. The photons in the idler arm are detected with polarization selection using a single photon counting module (SPCM) (Excelitas-

SPCM-800-14-FC), and the detection signals are sent to herald signal photons' arrival on the SPAD camera. Meanwhile, the signal photons are sent through a 10-meter-long single-mode fiber to the imaging setup. A lens with a focal length of 75 mm and a 10x objective are used to focus the signal beam onto the metasurface. The hologram generated from the metasurface is imaged by the SPAD camera (SPAD512S) using a 10x objective and a lens with a focal length of 125 mm. The heralded image of the signal photons in Figs. 3(b) to 3(f) are all retrieved using 600 frames with external triggers from SPCM and with background white noise subtracted. The background is measured using the same triggering setting with blocked signal photons. Each frame spans 100 ms with a maximum of 255 photon counts in each pixel. Each trigger from the SPCM would turn on the camera for a detection window of 18 ns. With multiple triggers within one frame, the detection events in each triggered window would accumulate into one frame.

2. Experimental results without erasure

Here Fig. S1 shows the quantum holographic results with a rotating signal polarizer without the erasure effect, which show no variation in the intensity level and are evaluated as the dashed curves in Fig. 4(b).

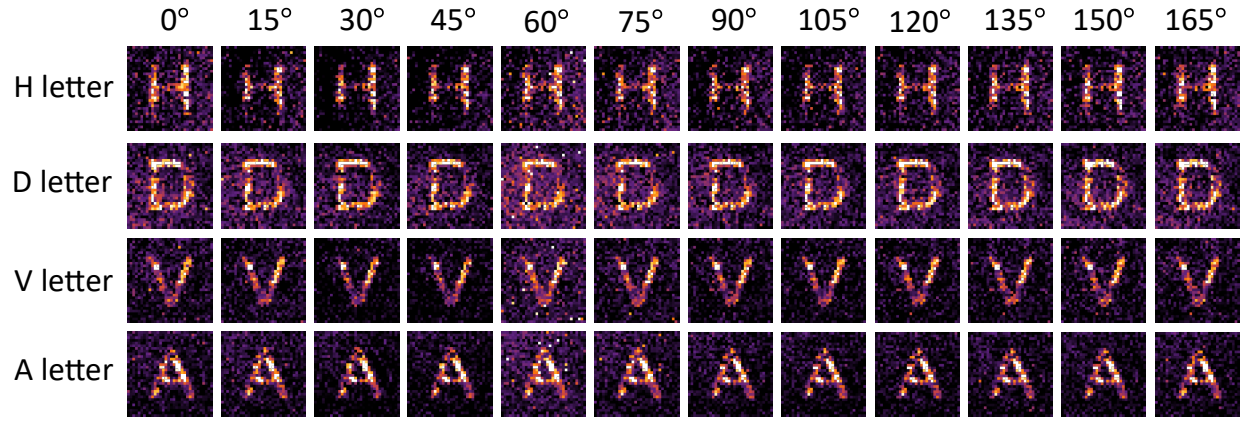

Fig. S1 Quantum hologram without the erasure effect.

3. Calculation of intensity drop, contrast, and Pearson correlation

To evaluate the erasure effect on the holographic results, we calculate the intensity drop, Pearson correlation, and contrast on the images. The intensity drop is defined as

$$\text{Intensity drop}_{i,j} = 10\log_{10}\left(I_{i,j}^{(\text{e})}/I_{i}^{(\text{w})}\right),$$

where $I_{i,j}^{(\text{e})} = I_{i,j}^{(\text{e,l})} - I_{i,j}^{(\text{e,b})}$ is the intensity of individual letter $i \in \{\text{H}, \text{D}, \text{V}, \text{A}\}$ of the hologram result j (a total of 4 results as shown in Figs. 3(c-f)) with erasure effect and is calculated as the difference between the average photon count of the letter $I_{i,j}^{(\text{e,l})}$ and the background $I_{i,j}^{(\text{e,b})}$ regions indicated as white and black regions in Fig. S2. Similarly, $I_{i}^{(\text{w})} = I_{i}^{(\text{w,l})} - I_{i}^{(\text{w,b})}$ is the intensity of the letter i of the hologram result without erasure. Then on average over the four holograms with erasure, the erased letters show a drop in intensity by -13.8 dB.

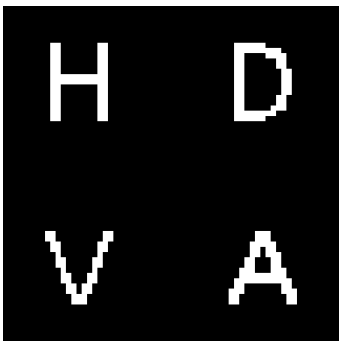

Fig. S2 The target holographic image as a mask to select letter and background regions.

For the remaining letters, we define the contrast for individual letters against the background as

$$\text{Contrast}_{i,j} = 10\log_{10}\left(\left(I_{i,j}^{(\text{e,l})} - I_{i,j}^{(\text{e,b})}\right)/I_{i,j}^{(\text{e,b})}\right),$$

and obtain an average contrast for the remaining letters as 7.5 dB. We further calculate the Pearson correlation coefficient for the remaining individual letter i between the result j with erasure and the result without erasure as

$$r_{i,j} = \frac{\sum_{x,y}(I_{i,j}^{(\text{e})}(x,y) - \bar{I}_{i,j}^{(\text{e})})(I_{i}^{(\text{w})}(x,y) - \bar{I}_{i}^{(\text{w})})}{\sqrt{\sum_{x,y}\left(I_{i,j}^{(\text{e})}(x,y) - \bar{I}_{i,j}^{(\text{e})}\right)^2}\sqrt{\sum_{x,y}\left(I_{i}^{(\text{w})}(x,y) - \bar{I}_{i}^{(\text{w})}\right)^2}},$$

where for example, $I_{i,j}^{(\text{e})}(x,y)$ is the intensity distribution for letter i, including its regional background, in the hologram result j with erasure. In this way, the remaining letters in all 4 results

with erasure show an average Pearson correlation coefficient of 0.64, demonstrating a high correlation. The above analysis suggests that despite the selective erasure of certain letters, the remaining holographic content retains sufficient clarity and coherence, facilitating effective interpretation.

4. High-dimension BB84 quantum key distribution implementation with holograms

In this section, we discuss the implementation of high-dimensional BB84 quantum key distribution using our metasurface-enabled quantum hologram platform. The BB84 protocol, first proposed by Bennett and Brassard in 1984 [55], is a quantum key distribution scheme for a sender, Alice, to generate and share a random private key with a receiver, Bob. In the original protocol, Alice and Bob first agree on two mutually unbiased bases (MUBs). Alice then randomly prepares quantum states in one of MUBs, while Bob randomly measures in either basis. After their quantum transmission, they publicly announce their basis choices and keep only the results where their bases are matched, allowing them to establish a secure key. Here, these MUBs are orthonormal bases $\{|\alpha_i\rangle\}$ and $\{|\beta_i\rangle\}$ such that $\left|\langle\alpha_i|\beta_j\rangle\right|^2 = 1/d$ for all i, j ranging from 1 to d where d is the dimension of the basis [53]. These bases are unbiased in the sense that a state prepared in one basis has an equal probability of being measured in any state of the other basis. For our high-dimensional implementation, we can construct MUBs using different spatial holographic states that satisfy this unbiased measurement probability condition. More specifically, possible choices of MUBs are

$$\{|\alpha_i\rangle\} = \{|H, \psi_R\rangle, |H, \psi_L\rangle, |V, \psi_R\rangle, |V, \psi_L\rangle\},$$

$$\{|\beta_i\rangle\} = \frac{1}{\sqrt{2}}\{|L, \psi_L\rangle + |R, \psi_R\rangle, |L, \psi_L\rangle - |R, \psi_R\rangle, |L, \psi_R\rangle + |R, \psi_L\rangle, |L, \psi_R\rangle - |R, \psi_L\rangle\},$$

where ψ_L and ψ_R are the LCP and RCP holograms in Fig. S.3 (a,b) chosen for simplicity of illustration. Given that two holograms are orthogonal to each other, i.e., $\langle\psi_L|\psi_R\rangle = 0$, these two bases satisfy the unbiased measurement probability condition for $d = 4$, i.e. $\left|\langle\alpha_i|\beta_j\rangle\right|^2 = 1/4$ for all i, j ranging from 1 to 4. Here, we define the (un-normalized) inner project of two spatial holographic states as $\langle\phi|\psi\rangle = \sum_{x,y} \phi^* \psi$ where both ϕ and ψ are any linear combination of the complex holographic field ψ_L and ψ_R.

It is important to note that the states $\{|\beta_i\rangle\}$ for all i are quantum holograms — these hybrid entangled states between polarization and spatial degrees of freedom offer extra flexibility in implementing BB84 QKD schemes which is enabled by our metasurface platform. For example,

Alice can generate all of these quantum hologram states with a new phase profile on the metasurface and make suitable adjustments to the angles of polarizers, half-wave plates, and quarter-wave plates. While our current implementation uses spatially separated holograms (ψ_L and ψ_R) to ensure orthogonality, the holographic states can be made more general due to our control of phase difference. As a simple example, we can construct another orthogonal states using superposition states such as $\psi_L \rightarrow \psi_L + \psi_R$ and $\psi_R \rightarrow \psi_L - \psi_R$. This demonstrates the flexibility of our platform in generating various orthogonal basis states for quantum key distribution.

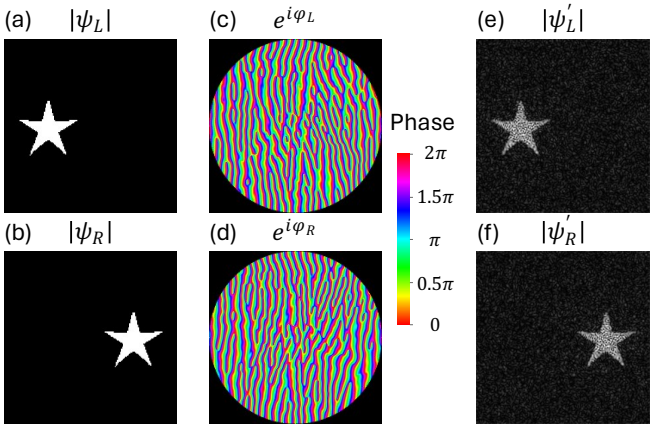

Fig. S3 (a, b) The orthogonal modes ψ_L, ψ_R for implementing high-dimensional BB84. (c, d) Phase maps generated by GS algorithm to realise the orthogonal modes in (a, b). (e, f) Estimated orthogonal modes ψ_L', ψ_R' after accounting for fabrication imperfections.

To numerically characterize our implementation, we use Gerchberg–Saxton (GS) algorithm to design two phase profiles $e^{i\varphi_L}, e^{i\varphi_R}$ as shown in Fig. S3 (c, d) such that $\mathrm{FT}(e^{i\varphi_{L/R}}) = \psi_{L/R}$. Here we assume that Alice is using a metasurface to independently control the phase and hologram for LCP and RCP [6]. To account for fabrication imperfections, we also add random phase profiles $e^{i\theta_{\mathrm{ran}}^{(L)}}$ and $e^{i\theta_{\mathrm{ran}}^{(R)}}$ to the metasurface with $\theta_{\mathrm{ran}}^{(L)}, \theta_{\mathrm{ran}}^{(R)}$ following normal distribution with 0 mean and $\pi/2$ standard deviation. After accounting for this imperfection, we denote the imperfect state as $|\alpha_i'\rangle$ and $|\beta_i'\rangle$ with the spatial modes $\psi_{L/R}$ replaced by $\psi_{L/R}' = \mathrm{FT}\left(e^{i\varphi_{L/R}} e^{i\theta_{\mathrm{ran}}^{(L/R)}}\right)$.

Next, we evaluate the crosstalk matrix $C_{ij} = \left\{\left|\langle\gamma_j|\gamma_i'\rangle\right|^2\right\}$ where $|\gamma_i\rangle = |\alpha_i\rangle$ for $i \leq 4$ and $|\gamma_i\rangle = |\beta_{i-4}\rangle$ for $i > 4$. This matrix captures all possible combinations of states prepared by Alice and their corresponding measurements by Bob. Here, Bob is projecting the spatial modes into two

perfect bases $\langle\alpha_i|$ and $\langle\beta_i|$. While the exact implementation of projecting onto the $\langle\beta_i|$ basis requires further development, falling outside the scope of the current work, we note that similar hybrid entanglement projections have been demonstrated in [51], where holograms were replaced by OAM modes, using q-plates and spatial light modulators for mode-selective detection. We also normalized each set of projections by Bob, which means the first four and last four elements for each row are normalized separately:

	$\langle\alpha_1\|$	$\langle\alpha_2\|$	$\langle\alpha_3\|$	$\langle\alpha_4\|$	$\langle\beta_1\|$	$\langle\beta_2\|$	$\langle\beta_3\|$	$\langle\beta_4\|$
$\|\alpha_1'\rangle$	0.983	0.017	0	0	0.311	0.189	0.311	0.189
$\|\alpha_2'\rangle$	0.009	0.991	0	0	0.295	0.205	0.295	0.205
$\|\alpha_3'\rangle$	0	0	0.983	0.017	0.189	0.311	0.189	0.311
$\|\alpha_4'\rangle$	0	0	0.009	0.991	0.205	0.295	0.205	0.295
$\|\beta_1'\rangle$	0.324	0.281	0.234	0.160	0.983	0.004	0.013	0.001
$\|\beta_2'\rangle$	0.234	0.160	0.324	0.281	0.004	0.983	0.001	0.013
$\|\beta_3'\rangle$	0.324	0.281	0.234	0.160	0.013	0.001	0.983	0.004
$\|\beta_4'\rangle$	0.234	0.160	0.324	0.281	0.001	0.013	0.004	0.983

From the results, we obtain a quantum bit error rate (QBER), $E = 1.50\%$, calculated as one minus the average of the diagonal elements in this crosstalk matrix. This error rate is below the error security threshold of 18% [54] (compared to 11% for two-dimensional BB84 QKD) which indicates the security of high-dimensional QKD using quantum holograms. Certainly, in an actual experiment (rather than numerical results here), E will be higher, but the increase of the security threshold due to the higher dimensional implementation helps the security of the protocol. Another measure is the mutual information between Alice and Bob, given by

$$I_{AB} = \log_2(d) + (1-E)\log_2(1-E) + E\log_2\left(\frac{E}{d-1}\right),$$

where $d = 4$ is the dimension of the basis. By substituting the numerical value of E, we obtain the mutual information as 1.86 bit (compared to maximally 1 bit for two-dimensional BB84 QKD). This result demonstrates that high-dimensional encoding using quantum holograms offers advantages over two-dimensional protocols [52]. We note that quantum hologram approach can be further extended to an even higher dimension than above results, e.g., through implementations using Jones matrix metasurfaces (more in-out polarization combinations) or metasurface lens-array designs (more path degrees of freedom), with corresponding benefits in higher data capacity and security thresholds. This enhanced dimensionality leads to more robust QKD implementations, as higher-dimensional quantum hologram schemes can tolerate larger quantum bit error rates while maintaining security. These results establish the quantum hologram as a more flexible basis in

high-dimensional quantum key distribution, offering a practical path toward enhanced quantum communication protocols.